

Anomalous energy transport and symmetry breaking in microscopic power grids

Julian Huber¹ and Peter Rabl¹

¹Vienna Center for Quantum Science and Technology, Atominstut, TU Wien, 1040 Vienna, Austria

(Dated: May 6, 2022)

We study the transport of energy through a microscopic network of coupled harmonic oscillators, where energy is injected at one end and extracted at the other end with finite rates. We evaluate the resulting energy currents under the influence of both thermal and quantum noise and describe various transport phenomena that arise from the competition between coherent and incoherent processes and the presence of nonlinear saturation effects. Specifically, we show that such networks exhibit a non-equilibrium phase transition between a noise-dominated and a coherent transport regime. This transition is associated with the formation and breaking of spatial symmetries, which is identified as a generic mechanism that affects many transport properties of active networks. Therefore, our findings have important practical consequences for the distribution of energy over coherent microwave, optical or phononic channels, in particular close to or at the quantum limit.

Motivated by fundamental thermodynamical considerations as well as potential practical applications, there has recently been a growing interest in the ultimate limits that determine the operation of generators, engines or refrigerators at the microscale, down to the level where such machines are realized by single quantum systems [1–5]. However, while many theoretical [6–21] and first experimental [22–28] studies about individual quantum machines have already been performed, there is still little known about interfacing multiple such devices. For example, how can the energy output of a microscopic generator be efficiently delivered to a microscopic engine and how will even larger networks of active quantum machines behave? Compared to conventional transmission lines for electric power, energy can be distributed at the microscale via highly coherent nanophotonic, microwave, or micromechanical channels. At the same time the influence of thermal and quantum fluctuations becomes important and thus the flow of energy through microscopic networks can differ strongly from Ohm's or Fourier's law.

In this work we analyze the active transfer of energy through a minimal ‘power grid’, which consists of a chain of coupled harmonic oscillators, as depicted in Fig. 1. Here energy is incoherently injected at one end and extracted at the other end of the chain, while the network is otherwise only very weakly coupled to the environment. To mimic microscopic generators and engines, we consider a finite saturation occupation number n_0 , which limits the maximal rate at which energy quanta can be emitted and absorbed. This parameter allows us to tune the degree of microscopcity of the network between the macroscopic, the thermal and the quantum regime. Despite its simplicity, this network already exhibits several surprising features. Most importantly, we find that there exist two basic modes of transport, which are separated by a sharp phase transition and differ strongly in their noise characteristics. This transition is accompanied by a change of the symmetry of the steady state, in close analogy to the phenomenon of \mathcal{PT} -symmetry breaking [30–35] in systems with equal gain and loss. Here we

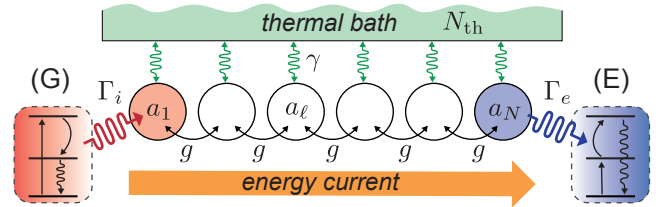


FIG. 1. Sketch of a microscopic power grid realized by an array of coupled harmonic oscillators. Energy is injected at one end by a microscopic generator (G) with rate Γ_i and extracted at the other end by a microscopic engine (E) with rate Γ_e . All oscillators are coupled weakly to a thermal environment. See text for more details.

show that the formation and breaking of spatial symmetries plays a much more general role for energy transport in coherent networks, even in systems where such symmetries are not reflected in the underlying equations of motion. Therefore, our findings have direct practical consequences for energy-distribution schemes at the microscopic level, but also reveal an interesting fundamental connection between non-equilibrium phase transitions and the operation of coupled networks of quantum machines.

Model.—We consider a chain of $N \geq 2$ coupled harmonic oscillators, as schematically shown in Fig. 1. The oscillators have a frequency ω_0 and they are coupled to their neighbors with strength g . Energy is injected at the first site with a rate Γ_i and extracted at the other end of the chain with rate Γ_e . In addition, all oscillators are weakly coupled to a thermal environment at temperature T . In the frame rotating with ω_0 , the dynamics of the whole chain is described by a master equation for the system density operator ρ ,

$$\begin{aligned} \dot{\rho} = & -\frac{i}{\hbar}[H_g, \rho] + \Gamma_i \mathcal{D}[A_1^\dagger] \rho + \Gamma_e \mathcal{D}[A_N] \rho \\ & + \sum_{\ell=1}^N \gamma (N_{\text{th}} + 1) \mathcal{D}[a_\ell] \rho + \gamma N_{\text{th}} \mathcal{D}[a_\ell^\dagger] \rho. \end{aligned} \quad (1)$$

Here a_ℓ (a_ℓ^\dagger) are the annihilation (creation) operators for each oscillator and $\mathcal{D}[a]\rho \equiv a\rho a^\dagger - (a^\dagger a\rho - \rho a^\dagger a)/2$. The first term in Eq. (1), where $H_g = -\frac{\hbar g}{2} \sum_{\ell=1}^{N-1} (a_\ell^\dagger a_{\ell+1} + \text{H.c.})$, describes the coherent exchange of energy between the oscillators, while the second and the third term model the incoherent pump and dissipation processes, respectively. The nonlinear jump operators $A_{\ell=1,N} = f(a_\ell^\dagger a_\ell) a_\ell$, where $f(0) = 1$ and $f(x \gg n_0) \rightarrow 0$, account for the fact that both the injection as well as the extraction of energy saturate above a characteristic occupation number n_0 . For concreteness we will focus here on the cutoff function

$$f(a^\dagger a) = \frac{1}{(1 + a^\dagger a/n_0)}, \quad (2)$$

which reproduces the saturation dependence of driven three-level generators and engines (see Fig. 1) [36]. However, none of the central results of this work depends on the precise shape of $f(x)$ and different functions can be used to model various other types of quantum machines [6–21]. Finally, the second line of Eq. (1) describes the coupling to the thermal bath with rate γ and equilibrium occupation number $N_{\text{th}} = (e^{\hbar\omega_0/k_B T} - 1)^{-1}$.

In the semiclassical regime, $n_0 \gg 1$, Eq. (1) can be mapped onto a Fokker-Planck equation for the Glauber-Sudarshan P-distribution $P(\{\alpha_\ell\}, t)$ [37, 38], which can be sampled efficiently by numerically integrating the corresponding stochastic Ito equations for the amplitudes α_ℓ (for details see [39, 40]),

$$\dot{\alpha}_1 = \frac{\Gamma_i(\alpha_1) - \gamma}{2} \alpha_1 + i\frac{g}{2} \alpha_2 + \sqrt{D_{\text{th}} + \Gamma_i(\alpha_1)} \xi_1(t), \quad (3)$$

$$\dot{\alpha}_\ell = -\frac{\gamma}{2} \alpha_\ell + i\frac{g}{2} (\alpha_{\ell-1} + \alpha_{\ell+1}) + \sqrt{D_{\text{th}}} \xi_\ell(t), \quad (4)$$

$$\dot{\alpha}_N = -\frac{\Gamma_e(\alpha_N) + \gamma}{2} \alpha_N + i\frac{g}{2} \alpha_{N-1} + \sqrt{D_{\text{th}}} \xi_N(t). \quad (5)$$

Here $\Gamma_{i,e}(\alpha) = \Gamma_{i,e} f^2(|\alpha|^2)$ and $D_{\text{th}} = \gamma N_{\text{th}}$ is the thermal diffusion rate. The $\xi_\ell(t)$ are white noise processes which satisfy $\langle \xi_\ell(t) \xi_{\ell'}(t') \rangle = \delta_{\ell\ell'} \delta(t-t')$. In this work, we are primarily interested in the steady-state energy current $\langle J_\ell \rangle = i\frac{g}{2} \langle a_\ell^\dagger a_{\ell-1} - a_{\ell-1}^\dagger a_\ell \rangle = g \text{Im} \langle \alpha_{\ell-1}^* \alpha_\ell \rangle$, which can be obtained from the longtime average over many trajectories, denoted by $\langle \langle \cdot \rangle \rangle$. In the regime of interest, $\gamma \rightarrow 0$, the average current is approximately constant throughout the chain and we can drop the index ℓ .

Anomalous energy transport. We first consider the macroscopic regime $n_0 \gg 1$ and $N_{\text{th}} \ll n_0$, where both thermal and quantum noise effects in Eqs. (3)–(5) can be neglected. The steady state of the network is then described by the set of amplitudes α_ℓ^0 and in Fig. 2(a) we plot the corresponding current $\langle J \rangle$ for $N = 10$ sites and different values of Γ_i and Γ_e . From this plot we already see that transport in this system is very different from Ohm's law, but also from the *passive* flow of heat through a coupled chain of linear oscillators [41]. Overall, we find regimes of normal transport, where for fixed

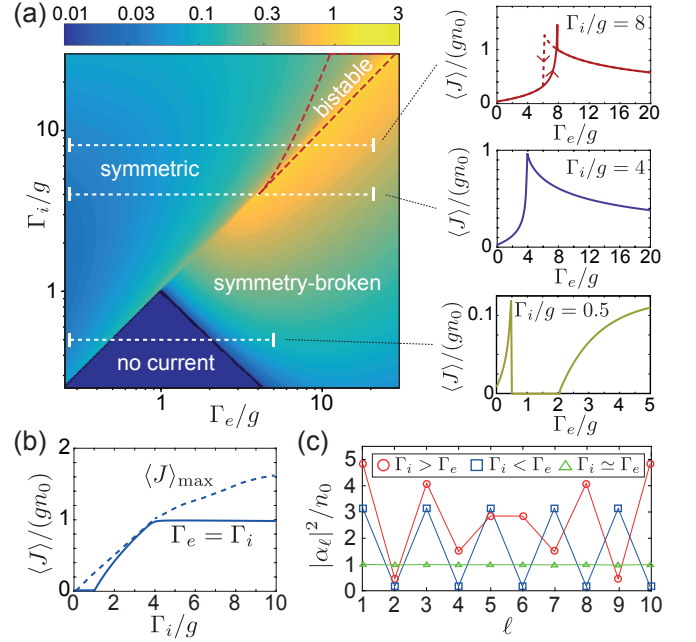


FIG. 2. (a) Plot of the normalized average current $\langle J \rangle / (gn_0)$ through a chain of $N = 10$ oscillators for different energy injection and extraction rates Γ_i and Γ_e . (b) For a given rate Γ_i the current $\langle J \rangle$ under symmetric conditions $\Gamma_e = \Gamma_i$ is compared with the maximal current $\langle J \rangle_{\text{max}}$, which is reached at a value $\Gamma_e = \Gamma_e^* = \Gamma_i - \mathcal{O}(\gamma)$. (c) The steady-state occupation numbers $|\alpha_\ell^0|^2$ of the whole chain are plotted in the symmetric ($\Gamma_i/\Gamma_e = 1.05$) and the symmetry-broken ($\Gamma_i/\Gamma_e = 2/3$) regime, as well as at the transition point, $\Gamma_e \simeq \Gamma_i$. For all plots $\gamma/g = 10^{-3}$ has been assumed.

Γ_i the current increases with increasing extraction rate Γ_e , but also regimes of anomalous transport, where the opposite behavior is observed. For $\Gamma_i < g$ there is a range of rates Γ_e , where the current is completely stalled and is only reestablished at higher extraction rates. This counterintuitive behavior [42, 43] can be traced back to the fact that within this specific parameter range all eigenvalues of the linear chain have a negative real part and the whole network is simply damped to zero [40]. At very high rates, $\Gamma_i/g > 4$, a bistable regime is found, where the value of the stationary current depends on the order in which the system is switched on. Leaving such metastable states aside, a sharp maximum of the current always occurs around $\Gamma_e \simeq \Gamma_i$. For $\Gamma_e = \Gamma_i$ the current then saturates at a value of $\langle J \rangle \simeq gn_0$ above the \mathcal{PT} -symmetry breaking point $\Gamma_i = \Gamma_e = 4g$ [34]. Note, however, that for $\gamma \rightarrow 0$ the current exhibits sharp spikes and discontinuities, where it jumps abruptly within the range $\delta\Gamma_e \sim \mathcal{O}(\gamma)$. Therefore, as shown in Fig. 2(b), the maximum current $\langle J \rangle_{\text{max}}$ for a given Γ_i , which for $N > 2$ and $\Gamma_i > g$ occurs at a value of about $\Gamma_e^* \simeq \Gamma_i(1 - N\gamma/(2g))$ [40] can even exceed the value of gn_0 , but only within a highly fine-tuned regime. We emphasize that this sharp maximum of the current around

$\Gamma_e \simeq \Gamma_i$ is not reflected in the eigenvalue structure of the linear chain [40] and is a feature of the active network with both saturable gain and loss.

Another interesting feature can be observed in Fig. 2(c), where we plot the steady-state occupation numbers $|\alpha_\ell^0|^2$. In contrast to conventional transport scenarios, the energy distribution along the chain exhibits an alternating zig-zag structure. For $\gamma \rightarrow 0$ and N even we obtain [40]

$$|\alpha_\ell^0|^2 = |A \sin(k_0 \ell) + B \cos(k_0 \ell)|^2, \quad (6)$$

where $k_0 = \pi/2(1 + 1/(N+1))$ for $\Gamma_i > \Gamma_e$ and $k_0 = \pi/2$ for $\Gamma_i < \Gamma_e$. Eq. (6) shows that the stationary current is carried by a single mode with wavevector $k_0 \approx \pi/2$, which is back-reflected at the extraction site and forms a standing wave. For $\Gamma_i > \Gamma_e$ the boundary condition is such that the two ends of the chain are symmetric, $|\alpha_1^0|^2 \simeq |\alpha_N^0|^2 \simeq |A|^2 \sim \sqrt{2(\Gamma_i - \Gamma_e)/(N\gamma)}$, and $B/A \sim -i\gamma/(\Gamma_i - \Gamma_e)$. For $\Gamma_i < \Gamma_e$ this symmetry is broken and $|\alpha_1^0|^2 \gg |\alpha_N^0|^2$. At the transition, where $\Gamma_e = \Gamma_e^*$, we obtain $B \simeq -iA$ and the transport becomes fully directional, $\alpha_\ell^0 \sim e^{ik_0 \ell} e^{-(\gamma/2g)\ell}$ [40].

Interestingly, for $\Gamma_i \neq \Gamma_e$ the symmetry in the steady state is emergent, i.e., it is not present in the underlying equations of motions. It also does not rely on the precise details of the saturation mechanism and is established as long as there is an amplitude α^0 , such that energy conservation $\Gamma_i(\alpha^0) - \Gamma_e(\alpha^0) \simeq \gamma N/2$ can be satisfied [40]. Only for larger chains this symmetry degrades, when either the bare damping, $N\gamma > g$, or too strong disorder prevents a ballistic transfer of excitations through the chain [40]. Therefore, consistent with studies of specific two-mode systems [32, 33], we find that the emergence of steady-state symmetries and the breaking thereof is a generic mechanism in active oscillator networks. The \mathcal{PT} -symmetric configuration, $\Gamma_i \simeq \Gamma_e$, then appears naturally as the phase boundary, along which additional symmetry-breaking transitions can take place [34].

Current fluctuations. To understand the actual consequences of this symmetry-breaking transition for microscopic transport, we consider now the thermal regime, $n_0 \gg 1$ and $N_{\text{th}} \sim n_0$. In this case quantum effects are still small, but noise from the environment can no longer be neglected and may induce strong fluctuations of the current, $\Delta J = \sqrt{\langle J^2 \rangle - \langle J \rangle^2}$. In thermal equilibrium $\Delta J = gN_{\text{th}}/\sqrt{2}$, which means that for $\Delta J/\langle J \rangle \sim N_{\text{th}}/n_0 > 1$, these thermal fluctuations exceed the average currents discussed above. In Fig. 3(a) we plot $\langle J \rangle$ and ΔJ for $N_{\text{th}}/n_0 = 10$ and for varying Γ_e . We see that in the symmetric phase transport is indeed dominated by fluctuations, which even exceed the thermal level. However, this behavior changes abruptly after the transition point $\Gamma_e \simeq \Gamma_i$, beyond which a well-defined current with a magnitude *below* the thermal noise level is established. This transition is also clearly visible

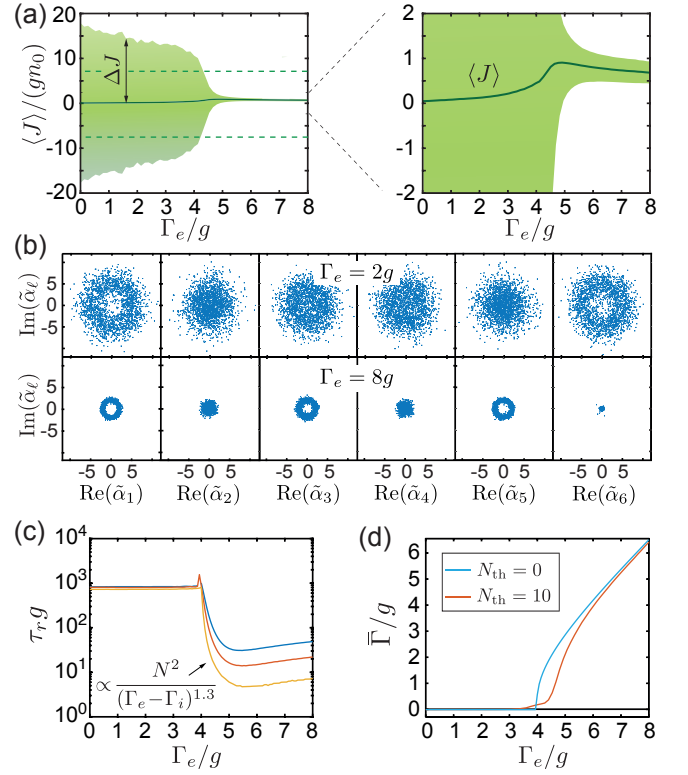


FIG. 3. (a) The average current $\langle J \rangle$ (solid line) and the current fluctuations ΔJ (shaded area) are plotted for a chain of $N = 6$ oscillators coupled to a thermal environment with $N_{\text{th}}/n_0 = 10$. The dashed lines indicate the range of current fluctuations in thermal equilibrium. The marginal phase space distributions $P_\ell(\alpha_\ell)$ are shown in (b) in the symmetric ($\Gamma_e = 2g$) and in the symmetry-broken ($\Gamma_e = 8g$) regime. Here $\tilde{\alpha}_\ell = \alpha_\ell/\sqrt{n_0}$. (c) Plot of the relaxation time τ_r as a function of Γ_e for $N = 4, 6, 8$ oscillators and $N_{\text{th}} = 0$. (d) The average dissipation rate $\bar{\Gamma} = \langle \Gamma_e(\alpha_N) - \Gamma_i(\alpha_1) \rangle$ in the absence and presence of thermal noise. In all plots a fixed value of $\Gamma_i/g = 4$ and $\gamma/g = 10^{-3}$ have been assumed.

in the steady-state distributions of the individual oscillators, $P_\ell(\alpha_\ell)$, shown in Fig. 3(b). For $\Gamma_i > \Gamma_e$ we observe strong fluctuations, but the distributions are still symmetric with respect to the center of the chain, i.e., $P_\ell \simeq P_{N-\ell+1}$. For $\Gamma_e > \Gamma_i$ this symmetry is broken and fluctuations are strongly suppressed.

The striking difference in the observed level of noise in the two phases can be related to an equivalent change in the response of the network. In Fig. 3(c) we plot the relaxation time τ_r , i.e., the time it takes for the amplitude α_1 to relax back into its steady-state value after a small perturbation [40]. In the symmetric phase, this time constant is approximately independent of Γ_i , Γ_e , and N . It is essentially determined by the bare damping rate, $\tau_r \sim \gamma^{-1}$, and diverges in the limit $\gamma \rightarrow 0$. In the symmetry-broken phase a much faster response, $\tau_r \sim O(\Gamma_e^{-1})$, and a scaling $\tau_r \sim N^2$ is observed. At the transition point the relaxation time diverges as

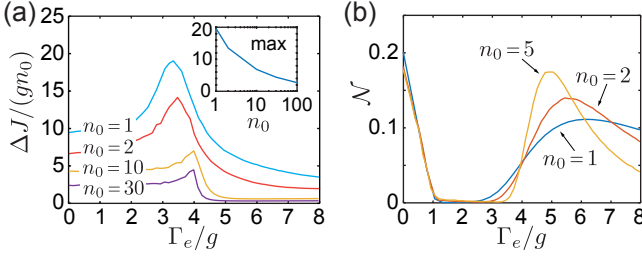


FIG. 4. (a) Plot of the current fluctuations ΔJ for $N = 2$ oscillators in the quantum noise limit $N_{\text{th}} = 0$ and for different saturation numbers $n_0 = 1, 2, 10, 30$. The inset shows the scaling of the maximum of the fluctuation peak as a function of n_0 . (b) Entanglement negativity \mathcal{N} of the steady-state density operator of the two coupled oscillators as a function of the loss strength Γ_e and $n_0 = 1, 2, 5$. For these plots a fixed injection rate $\Gamma_i/g = 4$ and a bare damping rate of (a) $\gamma/g = 10^{-3}$ and (b) $\gamma/g = 10^{-2}$ have been assumed. The results in this figure have been obtained from the semiclassical stochastic differential equations (3)-(5) for $n_0 \geq 10$ and from stochastic wavefunction simulations of the full density operator [40] for $n_0 = 1, 2, 5$.

$\tau_r \sim (\Gamma_e - \Gamma_i)^{-\xi}$, where from our numerical simulations we find $\xi \simeq 1.3$ for the saturation function in Eq. (2). Note that this behavior is very different from a laser or other non-equilibrium phase transitions, where the relaxation rate vanishes only at the transition point, but is finite and of similar magnitude in both phases [44–49]. Here the relaxation rate vanishes uniformly (in the limit $\gamma \rightarrow 0$) within the whole symmetric phase.

To provide an intuitive connection between the spatial symmetry of $P(\{\alpha_\ell\})$ and the current noise, it is useful to consider the mean damping rate $\bar{\Gamma} = \langle \Gamma_e(\alpha_N) - \Gamma_i(\alpha_1) \rangle$ [34], i.e., the difference between energy injection and extraction rates, averaged over the steady-state. In Fig. 3(d) we see that due to the symmetry of the marginal distributions for α_1 and α_N , this rate is vanishing small in the symmetric phase, $\bar{\Gamma} \sim O(\gamma)$. By breaking this symmetry, a finite positive value $\bar{\Gamma} \gg \gamma$ is established for $\Gamma_e > \Gamma_i$. This then leads—on average—to an efficient cooling of fluctuations and the possibility for subthermal energy transport. Therefore, the value of $\bar{\Gamma}$ represent a physically more meaningful order parameter than the symmetry of the steady state, which captures the transition between the noisy ($\Delta J \sim \gamma N_{\text{th}}/\bar{\Gamma} \sim N_{\text{th}}$) and the coherent ($\Delta J \sim \gamma N_{\text{th}}/\bar{\Gamma} \ll N_{\text{th}}$) transport regime [40].

Quantum noise limit. From Eq. (3) we see that even when the environment is cooled down to $N_{\text{th}} \approx 0$, the network is still affected by quantum noise $\sim \sqrt{\Gamma_i(\alpha_1)\xi_1(t)}$. In the regime $N_q = \Gamma_i/\gamma > N_{\text{th}}$, this noise dominates over thermal fluctuations and plays a fundamental role for energy transport deep in the quantum regime, $n_0 \sim O(1)$. Fig. 4(a) shows that for $n_0 \gg 1$, the sharp transition between a noisy and coherent transport regime still prevails in the limit $N_{\text{th}} = 0$. As the saturation

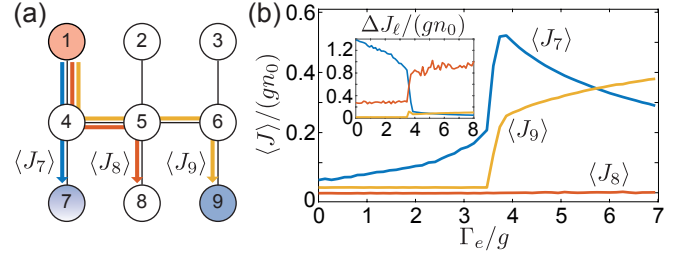


FIG. 5. (a) Sketch of a 2D power grid with multiple active sites. (b) Plot of the average currents $\langle J_\ell \rangle$ flowing from site 1 to sites $\ell = 7, 8, 9$ for fixed $\Gamma_i^{(1)}/g = \Gamma_e^{(9)}/g = 4$ and varying rate $\Gamma_e^{(7)}$. For this plot it is assumed that all oscillators are coupled to a thermal bath with a moderate occupation number $N_{\text{th}}/n_0 = 3$ and $\gamma/g = 10^{-3}$. The inset shows the resulting current fluctuations.

number n_0 is lowered, the relative level of fluctuations increases, develops a peak at the transition point and becomes much more pronounced also in the symmetry-broken phase. Note that for small $n_0 \lesssim 10$ the mapping of the master equation onto a Fokker-Planck equation is no longer valid and a full simulation of Eq. (1) must be performed [40]. Therefore, due to the large Hilbert space and large separation of time scales involved in such simulations, the results in Fig. 4 are restricted to $N = 2$ oscillators.

Access to the full density operator also allows us to investigate truly non-classical quantities, such as the steady-state entanglement established between the injection and extraction sites. In Fig. 4(b) we plot the entanglement negativity \mathcal{N} [40, 50, 51] as a function of Γ_e and for different saturation numbers $n_0 = 1, 2, 5$. We see that a significant amount of entanglement exists for $\Gamma_e < g$, it then vanishes in the remaining part of the symmetric phase, and peaks again around the transition point. Therefore, this plot reveals an additional substructure in the transport behavior, which is not reflected in the mean current or its fluctuations. The entanglement between source and drain can also be relevant for thermodynamical considerations, where not only the flow of energy, but also changes in entropy through mutual (quantum) correlations must be taken into account.

From power lines to power grids. The transport effects analyzed here in detail for a single channel will affect as well the flow of energy in more complex networks with multiple active sites. A basic example is illustrated in Fig. 5(a), where energy injected with rate $\Gamma_i^{(1)}$ at site 1 of a 2D grid is extracted at sites 7 and 9 with rates $\Gamma_e^{(7)}$ and $\Gamma_e^{(9)}$, respectively. Fig. 5(b) shows the resulting currents $\langle J_7 \rangle$ and $\langle J_9 \rangle$ for varying $\Gamma_e^{(7)}$. We see that although $\Gamma_e^{(9)} \gg \Gamma_e^{(7)}$, only a residual thermal current is initially flowing from site 1 to site 9. This behavior can be understood from the fact that a symmetric standing wave is formed between sites 1 and 7, which results in a

vanishing amplitude $\alpha_4 \approx 0$ at the crossing site. Once $\Gamma_e^{(7)}$ is increased above the value of about $\Gamma_i^{(1)}$, the symmetry breaks and $\alpha_4 \neq 0$ now supports a large current flowing to site 9. Simultaneously, we observe sharp jumps in the level of fluctuations, in analogy to the 1D chain. This example shows that due to interference and non-linear symmetry-breaking effects, currents in more complex networks can strongly influence each other in many non-intuitive ways. For the current network we obtain a transistor-like behavior, where a small increase of losses in one site leads to a sudden increase of the energy current through another part of the network.

Conclusion. In summary, we have described various energy-transport phenomena in coherent oscillator networks, which are representative for microscopic power grids connecting multiple quantum machines. As a generic feature we have discussed the emergence and breaking of spatial symmetries in the steady operation of such networks and showed that this mechanism affects transport properties in the macroscopic as well as deep in the quantum regime. These effects can be readily probed with state-of-the-art optomechanical [52], circuit QED [53] or trapped ion [54] systems, where various methods for engineered gain and loss processes at the quantum level are already experimentally available.

Acknowledgements.—We thank Stefan Rotter for stimulating discussions. This work was supported by the Austrian Science Fund (FWF) through the SFB FoQuS, Grant No. F40, the START Grant No. Y 591-N16, and the DK CoQuS, Grant No. W 1210.

-
- [1] D. Gelbwaser-Klimovsky, W. Niedenzu, and G. Kurizki, Thermodynamics of quantum systems under dynamical control, *Adv. At. Mol. Op. Phys.* **64**, 329 (2015).
 - [2] S. Vinjanampathy and J. Anders, Quantum thermodynamics, *Contemp. Phys.* **57**, 1 (2016).
 - [3] J. Goold, M. Huber, A. Riera, L. del Rio, and P. Skrzypczyk, The role of quantum information in thermodynamics — a topical review, *J. Phys. A: Math. Theor.* **49**, 143001 (2016).
 - [4] R. Alicki and R. Kosloff, Introduction to Quantum Thermodynamics: History and Prospects, *arXiv:1801.08314* (2018).
 - [5] J. Millen and A. Xuereb, Perspective: Quantum Thermodynamics, *New J. Phys.* **18**, 011002 (2016).
 - [6] H. E. D. Scovil, and E. O. Schulz-DuBois, Three-Level Masers as Heat Engines, *Phys. Rev. Lett.* **2**, 262 (1959).
 - [7] E. Geva and R. Kosloff, Three-level quantum amplifier as a heat engine: A study in finite-time thermodynamics, *Phys. Rev. E* **49**, 3903 (1994).
 - [8] M. O. Scully, M. S. Zubairy, G. S. Agarwal, and H. Walther, Extracting Work from a Single Heat Bath via Vanishing Quantum Coherence, *Science* **299**, 862 (2003).
 - [9] T. D. Kieu, The Second Law, Maxwell's Demon, and Work Derivable from Quantum Heat Engines, *Phys. Rev. Lett.* **93**, 140403 (2004).
 - [10] H. T. Quan, Y. xi Liu, C. P. Sun, and F. Nori, Quantum thermodynamic cycles and quantum heat engines, *Phys. Rev. E* **76**, 031105 (2007).
 - [11] N. Linden, S. Popescu, and P. Skrzypczyk, How Small Can Thermal Machines Be? The Smallest Possible Refrigerator, *Phys. Rev. Lett.* **105**, 130401 (2010).
 - [12] O. Abah, J. Ronagel, G. Jacob, S. Deffner, F. Schmidt-Kaler, K. Singer, and E. Lutz, Single-Ion Heat Engine at Maximum Power, *Phys. Rev. Lett.* **109**, 203006 (2012).
 - [13] D. Gelbwaser-Klimovsky, R. Alicki, and G. Kurizki, Minimal universal quantum heat machine, *Phys. Rev. E* **87**, 012140 (2013).
 - [14] R. Gallego, A. Riera, and J. Eisert, Thermal machines beyond the weak coupling regime, *New J. Phys.* **16**, 125009 (2014).
 - [15] K. Zhang, F. Bariani, and P. Meystre, Quantum Optomechanical Heat Engine, *Phys. Rev. Lett.* **112**, 150602 (2014).
 - [16] C. Bergenfeldt, P. Samuelsson, B. Sothmann, C. Flindt, and M. Büttiker, Hybrid Microwave-Cavity Heat Engine, *Phys. Rev. Lett.* **112**, 076803 (2014).
 - [17] M. Brunelli, A. Xuereb, A. Ferraro, G. De Chiara, N. Kiesel, and M. Paternostro, Out-of-equilibrium thermodynamics of quantum optomechanical systems, *New J. Phys.* **17**, 035016 (2015).
 - [18] C. Elouard, M. Richard, and A. Auffeves, Reversible work extraction in a hybrid opto-mechanical system, *New J. Phys.* **17**, 055018 (2015).
 - [19] A. Dechant, N. Kiesel, and E. Lutz, All-Optical Nanomechanical Heat Engine, *Phys. Rev. Lett.* **114**, 183602 (2015).
 - [20] A. Mari, A. Farace, and V. Giovannetti, Quantum optomechanical piston engines powered by heat, *J. Phys. B* **48**, 175501 (2015).
 - [21] S.-W. Li, M. B. Kim, G. S. Agarwal, and M. O. Scully, Quantum statistics of a single-atom heat engine, *Phys. Rev. A* **96**, 063806 (2017).
 - [22] T. Hugel, N. B. Holland, A. Cattani, L. Moroder, M. Seitz, and H. E. Gaub, Single-molecule optomechanical cycle, *Science* **296**, 1103 (2002).
 - [23] P. G. Steeneken, K. Le Phan, M. J. Goossens, G. E. J. Koops, G. J. A. M. Brom, C. van der Avoort, and J. T. M. van Beek, Piezoresistive heat engine and refrigerator, *Nature Phys.* **7**, 354 (2011).
 - [24] V. Blickle and C. Bechinger, Realization of a micrometre-sized stochastic heat engine, *Nature Phys.*, **8**, 143 (2012).
 - [25] J.-P. Brantut, C. Grenier, J. Meineke, D. Stadler, S. Krinner, C. Kollath, T. Esslinger, and A. Georges, A Thermoelectric Heat Engine with Ultracold Atoms, *Science* **342**, 713 (2013).
 - [26] H. Thierschmann, R. Sanchez, B. Sothmann, F. Arnold, C. Heyn, W. Hansen, H. Buhmann, and L. W. Molenkamp, Three-terminal energy harvester with coupled quantum dots, *Nat. Nanotechnol.* **10**, 854 (2015).
 - [27] J. Roßnagel, S. T. Dawkins, K. N. Tolazzi, O. Abah, E. Lutz, F. Schmidt-Kaler, and K. Singer, A single-atom heat engine, *Science* **352**, 325 (2016).
 - [28] F. Schmidt, A. Magazza, A. Callegari, L. Biancofiore, F. Cichos, and G. Volpe, Microscopic Engine Powered by Critical Demixing, *Phys. Rev. Lett.* **120**, 068004 (2018).
 - [29] J. Klaers, S. Faelt, A. Imamoglu, and E. Togan, Squeezed thermal reservoirs as a resource for a nano-mechanical engine beyond the Carnot limit, *Phys. Rev. X* **7**, 031044 (2017).

- [30] C. M. Bender and S. Boettcher, Real spectra in non-hermitian hamiltonians having PT symmetry, *Phys. Rev. Lett.* **80**, 5243 (1998).
- [31] R. El-Ganainy, K. G. Makris, M. Khajavikhan, Z. H. Musslimani, S. Rotter, and D. N. Christodoulides, Non-Hermitian physics and PT symmetry, *Nature Phys.* **14**, 11 (2018).
- [32] A. U. Hassan, H. Hodaei, M. A. Miri, M. Khajavikhan, and D. N. Christodoulides, Nonlinear reversal of the PT-symmetric phase transition in a system of coupled semiconductor microring resonators, *Phys. Rev. A* **92**, 63807 (2015).
- [33] L. Ge and R. El-Ganainy, Nonlinear modal interactions in parity-time (PT) symmetric lasers, *Sci. Rep.* **6**, 24889 (2016).
- [34] K. V. Kepesidis, T. J. Milburn, J. Huber, K. G. Makris, S. Rotter, and P. Rabl, PT-symmetry breaking in the steady state of microscopic gain-loss systems, *New J. Phys.* **18**, 095003 (2016).
- [35] S. Assawaworrarit, X. Yu, and S. Fan, Robust wireless power transfer using a nonlinear parity-time-symmetric circuit, *Nature* **546**, 387 (2017).
- [36] K. V. Kepesidis, S. D. Bennett, S. Portolan, M. D. Lukin, and P. Rabl, Phonon Cooling and Lasing with Nitrogen-Vacancy Centers in Diamond, *Phys. Rev. B* **88**, 064105 (2013).
- [37] D. F. Walls, and G. J. Milburn, *Quantum Optics* (Springer, 1994).
- [38] C. W. Gardiner and P. Zoller, *Quantum Noise* (Springer, 2000).
- [39] C. Gardiner, *Stochastic methods* (Springer, Berlin, 2009).
- [40] See Supplemental Material for the derivation of the main analytic results and for additional numerical examples.
- [41] A. Asadian, D. Manzano, M. Tiersch, and H. J. Briegel, Heat transport through lattices of quantum harmonic oscillators in arbitrary dimensions, *Phys. Rev. E* **87**, 012109 (2013).
- [42] B. Peng, S. K. Özdemir, S. Rotter, H. Yilmaz, M. Liertzer, F. Moni, C. M. Bender, F. Nori, and L. Yang, Loss-induced suppression and revival of lasing, *Science* **346**, 328 (2014).
- [43] M. Brandstetter, M. Liertzer, C. Deutsch, P. Klang, J. Schöberl, H. E. Türeci, G. Strasser, K. Unterrainer, and S. Rotter, Reversing the pump dependence of a laser at an exceptional point, *Nature Commun.* **5**, 4034 (2014).
- [44] S. Diehl, A. Tomadin, A. Micheli, R. Fazio, and P. Zoller, Dynamical Phase Transitions and Instabilities in Open Atomic Many-Body Systems, *Phys. Rev. Lett.* **105**, 015702 (2010).
- [45] D. Nagy, G. Szirmai, and P. Domokos, Critical exponent of a quantum-noise-driven phase transition: The open-system Dicke model, *Phys. Rev. A* **84**, 043637 (2011).
- [46] B. Öztop, M. Bordyuh, Ö. E. Müstecaploglu, and H. E. Türeci, Excitations of optically driven atomic condensate in a cavity: theory of photodetection measurements, *New J. Phys.* **14**, 085011 (2012).
- [47] E. M. Kessler, G. Giedke, A. Imamoglu, S. F. Yelin, M. D. Lukin, and J. I. Cirac, Dissipative phase transition in a central spin system, *Phys. Rev. A* **86**, 012116 (2012).
- [48] W. Casteels, F. Storme, A. LeBoite, and C. Ciuti, Power Laws in the Dynamic Hysteresis of Quantum Nonlinear Photonic Resonators, *Phys. Rev. A* **93**, 033824 (2016).
- [49] M.-J. Hwang, P. Rabl, and M. B. Plenio, Dissipative Phase Transition in the Open Quantum Rabi Model, *Phys. Rev. A* **97**, 013825 (2018).
- [50] K. Życzkowski, P. Horodecki, A. Sanpera, and M. Lewenstein, Volume of the set of separable states, *Phys. Rev. A* **58**, 883 (1998).
- [51] G. Vidal, and R. F. Werner, Computable measure of entanglement, *Phys. Rev. A* **65**, 032314 (2002).
- [52] M. Aspelmeyer, T. J. Kippenberg, and F. Marquardt, Cavity optomechanics, *Rev. Mod. Phys.* **86**, 1391 (2014).
- [53] X. Gu, A. Frisk Kockum, A. Miranowicz, Y.-X. Liu, and F. Nori, Microwave photonics with superconducting quantum circuits, *Phys. Rep.* **718**, 1 (2017).
- [54] D. Leibfried, R. Blatt, C. Monroe, and D. Wineland, Quantum dynamics of single trapped ions, *Rev. Mod. Phys.* **75**, 281 (2003).

**Supplementary material for:
Anomalous energy transport and symmetry breaking in microscopic power grids**

FOKKER-PLANCK EQUATION

In the main text we use master equation (1) as a starting point for our analysis. This equation describes the dynamics of the full system density operator ρ and can be written as

$$\dot{\rho} = (\mathcal{L}_{\text{lin}} + \mathcal{L}_{\text{nl}})\rho. \quad (\text{S1})$$

Here the first term,

$$\mathcal{L}_{\text{lin}}\rho = i \left[\sum_{\ell=1}^{N-1} \frac{g}{2} (a_{\ell}^{\dagger} a_{\ell+1} + a_{\ell} a_{\ell+1}^{\dagger}), \rho \right] + \sum_{\ell=1}^N \gamma (N_{\text{th}} + 1) \mathcal{D}[a_{\ell}]\rho + \gamma N_{\text{th}} \mathcal{D}[a_{\ell}^{\dagger}]\rho, \quad (\text{S2})$$

where $\mathcal{D}[a]\rho \equiv a\rho a^{\dagger} - (a^{\dagger}a\rho + \rho a^{\dagger}a)/2$, describes the linear dynamics of the passive chain, i.e., the coherent exchange of energy between neighboring oscillators and the coupling to the environment. The second term in Eq. (S1) accounts for the injection and the extraction of energy at the ends of the chain and is given by

$$\mathcal{L}_{\text{nl}}\rho = \Gamma_i \mathcal{D}[A_1^{\dagger}]\rho + \Gamma_e \mathcal{D}[A_N]\rho. \quad (\text{S3})$$

To include saturation effects while keeping the analysis as general as possible, we model these processes by non-linear jump operators $A_{\ell=1,N} = f(a_{\ell}^{\dagger} a_{\ell}) a_{\ell}$. For a given physical implementation, the cutoff function $f(x)$, which satisfies $f(0) = 1$ and $f(x \gg n_0) \rightarrow 0$, is chosen such that it reproduces the correct saturation dependence in the semi-classical regime (see below). For example, the choice

$$f(a^{\dagger} a) = \frac{1}{(1 + a^{\dagger} a/n_0)^{\nu/2}} \quad (\text{S4})$$

reproduces the saturation behavior of a regular two-level laser for $\nu = 1$ [S1, S2] and that of a driven three-level lasing or cooling process for $\nu = 2$ [S3].

In the semiclassical regime $n_0 \gg 1$ the cutoff function $f(x)$ varies slowly on the scale of individual excitations and the master equation can be mapped onto a Fokker-Planck equation for the Glauber-Sudarshan P-representation [S1, S2, S4]. This distribution function is defined by

$$\rho = \int \prod_{\ell} d^2\alpha_{\ell} P(\{\alpha_{\ell}\}) |\{\alpha_{\ell}\}\rangle \langle \{\alpha_{\ell}\}|, \quad (\text{S5})$$

where $|\{\alpha_{\ell}\}\rangle$ denotes a multi-component coherent state. By using the usual substitution rules [S1, S2]

$$a_{\ell}\rho \rightarrow \alpha_{\ell}P, \quad a_{\ell}^{\dagger}\rho \rightarrow \left(\alpha_{\ell}^* - \frac{\partial}{\partial \alpha_{\ell}} \right) P, \quad \rho a_{\ell}^{\dagger} \rightarrow \alpha_{\ell}^*P, \quad \rho a_{\ell} \rightarrow \left(\alpha_{\ell} - \frac{\partial}{\partial \alpha_{\ell}^*} \right) P, \quad (\text{S6})$$

we can convert Eq. (S1) for the density operator ρ into a partial differential equation for $P(\{\alpha_{\ell}\})$. We obtain

$$\frac{\partial P}{\partial t} = \frac{\partial P}{\partial t} \Big|_{\text{lin}} + \frac{\partial P}{\partial t} \Big|_{\text{nl}}, \quad (\text{S7})$$

where the first term,

$$\frac{\partial P}{\partial t} \Big|_{\text{lin}} = \frac{1}{2} \left[-ig \sum_{\ell=2}^{N-1} \left(\frac{\partial}{\partial \alpha_{\ell}} (\alpha_{\ell-1} + \alpha_{\ell+1}) - \frac{\partial}{\partial \alpha_{\ell}^*} (\alpha_{\ell-1}^* + \alpha_{\ell+1}^*) \right) + \gamma \sum_{\ell=1}^N \left(\frac{\partial}{\partial \alpha_{\ell}} \alpha_{\ell} + \frac{\partial}{\partial \alpha_{\ell}^*} \alpha_{\ell}^* + 2N_{\text{th}} \frac{\partial^2}{\partial \alpha_{\ell} \partial \alpha_{\ell}^*} \right) \right] P, \quad (\text{S8})$$

describes the linear chain and already has the form of a Fokker-Planck equation.

The second term in Eq. (S7) contains higher order derivatives, which are generated by the nonlinear dissipative terms in Eq. (S3), and additional approximations are required. To do so we first use the substitution rules from above

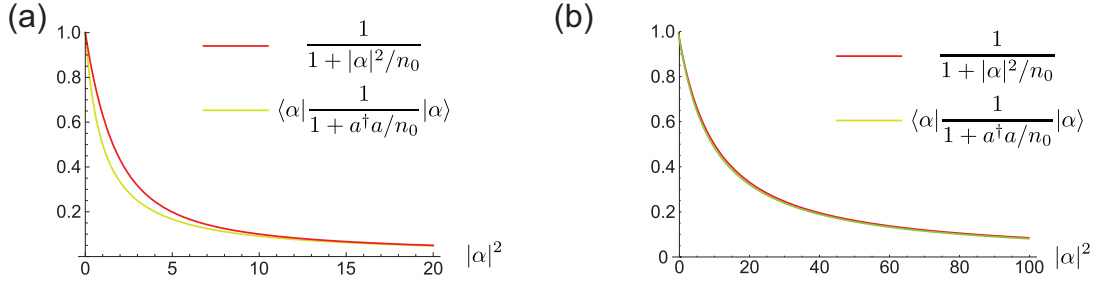


FIG. S1. Plot of the function $\bar{f}(\alpha, \alpha^*) = \langle \alpha | \frac{1}{1+a^\dagger a/n_0} | \alpha \rangle$ and its approximated form $\frac{1}{1+|\alpha|^2/n_0}$ for (a) $n_0 = 1$ and (b) $n_0 = 10$.

to translate the action of $f(a^\dagger a)$ on the density operator into a differential operator for the P-distribution (omitting the site index),

$$f(a^\dagger a)\rho \rightarrow \sum_{m=0}^{\infty} \bar{f}_m \alpha^m \left(\alpha^* - \frac{\partial}{\partial \alpha} \right)^m P(\alpha, \alpha^*). \quad (\text{S9})$$

Here the coefficients \bar{f}_m follow from an expansion of the operator $f(a^\dagger a)$ into a normally ordered series

$$f(a^\dagger a) = \sum_{m=0}^{\infty} \bar{f}_m (a^\dagger)^m a^m. \quad (\text{S10})$$

By using the binomial theorem

$$\left(\alpha^* - \frac{\partial}{\partial \alpha} \right)^m = \sum_{k=0}^m \binom{m}{k} (\alpha^*)^{m-k} (-1)^k \frac{\partial^k}{\partial \alpha^k} = \sum_{k=0}^m \frac{(-1)^k}{k!} \frac{\partial^k}{\partial \alpha^{*k}} (\alpha^{*m}) \frac{\partial^k}{\partial \alpha^k}, \quad (\text{S11})$$

we arrive at

$$f(a^\dagger a)\rho \rightarrow \sum_{m=0}^{\infty} \sum_{k=0}^m \bar{f}_m \alpha^m \frac{(-1)^k}{k!} \frac{\partial^k}{\partial \alpha^{*k}} (\alpha^{*m}) \frac{\partial^k}{\partial \alpha^k} P(\alpha) = \sum_{k=0}^{\infty} \frac{(-1)^k}{k!} \frac{\partial^k}{\partial \alpha^{*k}} [\bar{f}(\alpha, \alpha^*)] \frac{\partial^k}{\partial \alpha^k} P(\alpha, \alpha^*), \quad (\text{S12})$$

where $\bar{f}(\alpha, \alpha^*) = \langle \alpha | f(a^\dagger a) | \alpha \rangle$. Since $f(a^\dagger a)$ is a function of $a/\sqrt{n_0}$ and $a^\dagger/\sqrt{n_0}$, the derivatives of $\bar{f}(\alpha, \alpha^*)$ scale as $\frac{\partial^k}{\partial \alpha^{*k}} \bar{f}(\alpha, \alpha^*) \propto n_0^{-k/2}$. Therefore, in the limit $n_0 \rightarrow \infty$, we can neglect all derivatives and approximate

$$f(a^\dagger a)\rho \rightarrow \bar{f}(\alpha, \alpha^*) P(\alpha, \alpha^*) + \mathcal{O}\left(\frac{1}{\sqrt{n_0}}\right). \quad (\text{S13})$$

Note that the definition of $\bar{f}(\alpha, \alpha^*)$ is based on the normally ordered series expansion and in general $\bar{f}(\alpha, \alpha^*) \neq f(|\alpha|^2)$. Therefore, in our derivation we make a second approximation and neglect this difference, i.e.,

$$\bar{f}(\alpha, \alpha^*) = \langle \alpha | \frac{1}{1+a^\dagger a/n_0} | \alpha \rangle \approx \frac{1}{1+|\alpha|^2/n_0}. \quad (\text{S14})$$

To show the validity of this approximation, we compare in Fig. (S1) the function $\langle \alpha | \frac{1}{1+a^\dagger a/n_0} | \alpha \rangle = e^{-|\alpha|^2} (-|\alpha|)^{-n_0} [\Gamma(n_0, 0) - \Gamma(n_0, -|\alpha|^2)]$ [S6] with the approximate form $\frac{1}{1+|\alpha|^2/n_0}$. Here Γ denotes the incomplete Gamma function. We see that even deep in the quantum regime, $n_0 \approx 1$, this second approximation only leads to a small correction, which become negligible for $n_0 \gtrsim 10$. Therefore, we conclude that the main approximation in the derivation of our semiclassical Fokker-Planck equation comes from neglecting higher order derivatives in Eq. (S12).

Based on these considerations we obtain the following approximate substitution rules

$$A\rho \rightarrow \frac{\alpha}{(1+|\alpha|^2/n_0)} P(\alpha, \alpha^*), \quad A^\dagger \rho \rightarrow \left(\alpha^* - \frac{\partial}{\partial \alpha} \right) \frac{1}{(1+|\alpha|^2/n_0)} P(\alpha, \alpha^*), \quad (\text{S15})$$

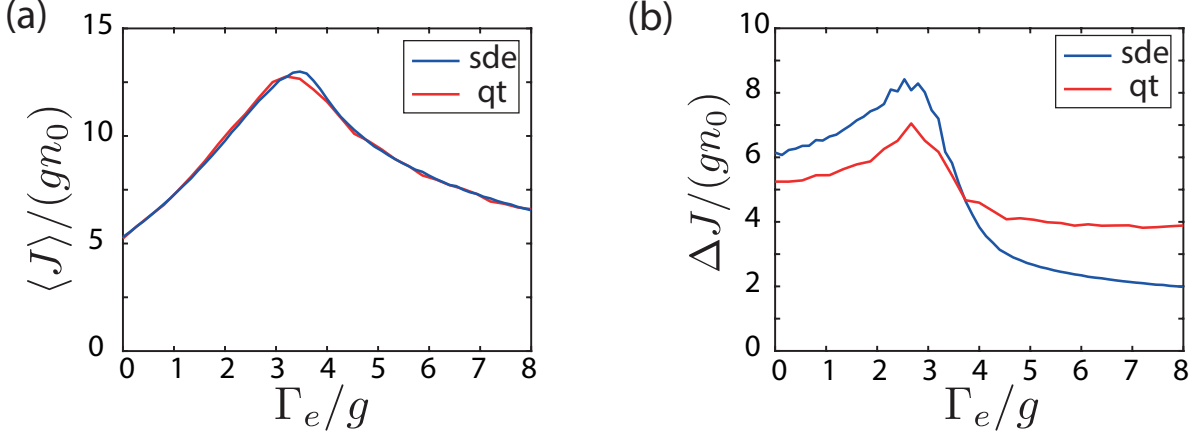


FIG. S2. Comparison of (a) the mean current and (b) the current fluctuations as obtained from quantum trajectory (qt) simulations of the full master equation and from the semiclassical stochastic differential (sde) equations. For both plots $n_0 = 15$, $\gamma/g = 10^{-1}$ and $\Gamma_i = 4g$.

and analogous relations for ρA and ρA^\dagger . All together we then obtain

$$\begin{aligned} \left. \frac{\partial P}{\partial t} \right|_{\text{nl}} = & \frac{1}{2} \left[-\frac{\partial}{\partial \alpha_1} \Gamma_i(\alpha_1) \alpha_1 - \frac{\partial}{\partial \alpha_1^*} \Gamma_i(\alpha_1) \alpha_1^* + 2 \frac{\partial^2}{\partial \alpha_1 \partial \alpha_1^*} \Gamma_i(\alpha_1) \right. \\ & \left. + \frac{\partial}{\partial \alpha_N} \Gamma_e(\alpha_N) \alpha_N + \frac{\partial}{\partial \alpha_N^*} \Gamma_e(\alpha_N) \alpha_N^* \right] P, \end{aligned} \quad (\text{S16})$$

where $\Gamma_{i,e}(\alpha) = \Gamma_{i,e} f^2(|\alpha|^2)$.

We see that after these approximations the P-distribution in the limit $n_0 \gg 1$ obeys a Fokker-Planck equation. Therefore, it can be sampled efficiently using the corresponding set of stochastic differential equations (3)-(5) in the main text [S5]. To judge the validity of this approximation also for moderate n_0 , we compare in Fig. (S2) the numerical solution of the full master equation (S1) using quantum trajectories (see Sec. below) with the semiclassical stochastic differential equations. For this plot we have assumed $n_0 = 15$, but a value of $\gamma/g = 10^{-1}$ to limit the number of basis states in the exact simulation. This comparison shows that there are hardly any differences in the mean current and that also the current fluctuations are qualitatively well reproduced. Note that for smaller values of γ , as used in the main text, the oscillator amplitudes are higher and an even better agreement is expected.

LINEAR CHAIN

In Fig. (S3) we plot the largest real part of all the eigenvalues obtained from the dynamical matrix of a linear chain where $\Gamma_{i,e}(\alpha) = \Gamma_{i,e}$. As long as all eigenvalues have a negative real part, the chain is damped to zero. This only occurs in the ‘stalled’ phase where $\Gamma_i < g$ and $\Gamma_i \leq \Gamma_e < g^2/\Gamma_i$. Otherwise, we see that the structure of the current plotted in Fig. 2(a) in the maintext is not at all reflected in the eigenvalue structure of the linear chain.

STEADY STATE AMPLITUDES

In the limit $n_0 \gg 1$ and $N_{\text{th}}/n_0 \rightarrow 0$, the stochastic terms in Eqs. (3)-(5) in the main text can be neglected and we obtain a set of ordinary differential equations with steady-state amplitudes α_ℓ^0 . To obtain analytic insights about the steady state of the chain in this regime, we consider in the following the slightly simplified scenario, where only sites $\ell = 1$ and $\ell = N$ are affected by the bare decay $\gamma/g \ll 1$, while all the other oscillators evolve coherently.

We are interested in the long-time dynamics of the chain and make the following ansatz for the amplitudes

$$\alpha_\ell^0(t) = \sqrt{n_0} e^{-i\omega t} [A \sin(k_0 \ell) + B \cos(k_0 \ell)], \quad (\text{S17})$$

where $A, B \in \mathbb{C}$ and $\omega = g \cos(k_0)$. With this ansatz the current between two sites is

$$\langle J_\ell \rangle = g \text{Im}\{(\alpha_{\ell-1}^0)^* \alpha_\ell^0\} = gn_0 \text{Im}\{AB^*\} \sin(k_0). \quad (\text{S18})$$

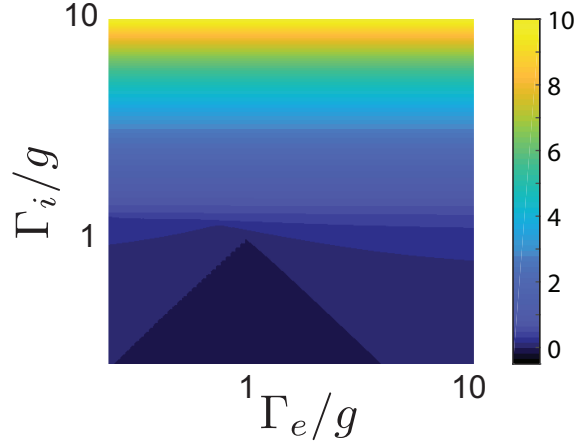


FIG. S3. Plot of the largest real part of the eigenvalues of a linear chain of $N = 10$ oscillators with a damping rate $\gamma = 10^{-3}g$.

To obtain a steady state configuration which maximizes the energy transfer we look for solutions with k_0 equal or close to $\pi/2$. By writing $k_0 = \pi/2 + \delta$ we obtain the equation

$$\left[\frac{\Gamma_i/2}{(1 + |A \cos(\delta) - B \sin(\delta)|^2)^2} - \frac{\gamma}{2} \right] (A \cos(\delta) - B \sin(\delta)) - i \frac{g}{2} B = 0, \quad (\text{S19})$$

from the equation of motion for α_1 . Similarly, from the equation of motion for α_N we obtain

$$\begin{aligned} \left[-\frac{\Gamma_e/2}{(1 + |-A \cos(\delta N) + B \sin(\delta N)|^2)^2} - \frac{\gamma}{2} \right] (-A \cos(\delta N) + B \sin(\delta N)) \\ - i \frac{g}{2} (A \sin(\delta(N+1)) + B \cos(\delta(N+1))) = 0, \end{aligned} \quad (\text{S20})$$

for the case where N is odd and

$$\begin{aligned} \left[-\frac{\Gamma_e/2}{(1 + |A \sin(\delta N) + B \cos(\delta N)|^2)^2} - \frac{\gamma}{2} \right] (A \sin(\delta N) + B \cos(\delta N)) \\ - i \frac{g}{2} (A \cos(\delta(N+1)) - B \sin(\delta(N+1))) = 0, \end{aligned} \quad (\text{S21})$$

for the case where N is even. To proceed with our analysis we must distinguish between the symmetric ($\Gamma_i > \Gamma_e$) and the symmetry-broken regime ($\Gamma_e > \Gamma_i$) and between an even and an odd number of oscillators.

Symmetric phase

We first consider the regime $\Gamma_i > \Gamma_e$ and N odd. In this case the choice $k_0 = \pi/2$ results in $\omega = 0$ and a symmetric solution for the amplitudes, $|\alpha_1^0| = |\alpha_N^0|$. The remaining parameters A and B are determined by the two coupled equations

$$\left(\frac{\Gamma_i}{(1 + |A|^2)^2} - \gamma \right) A - igB = 0, \quad (\text{S22})$$

$$\left(\frac{-\Gamma_e}{(1 + |A|^2)^2} - \gamma \right) A + igB = 0. \quad (\text{S23})$$

For $\Gamma_e < \Gamma_i - 2\gamma$, there exists the solution

$$|A|^2 = \sqrt{\frac{\Gamma_i - \Gamma_e}{2\gamma}} - 1, \quad B = -i \frac{\gamma}{g} \frac{\Gamma_i + \Gamma_e}{\Gamma_i - \Gamma_e} A, \quad (\text{S24})$$

and for the current we obtain

$$\langle J \rangle = n_0 \gamma \frac{\Gamma_i + \Gamma_e}{\Gamma_i - \Gamma_e} \left(\sqrt{\frac{\Gamma_i - \Gamma_e}{2\gamma}} - 1 \right). \quad (\text{S25})$$

For N even, the choice $k_0 = \pi/2$ would results in an asymmetric steady-state and also the resulting equations for A and B do not have a solution for $\Gamma_i > \Gamma_e$. To recover a symmetric solution with a maximal current we choose $\delta = \pi/(2(N+1))$. In this case the chain undergoes persistent oscillations with frequency $\omega = g \sin(\delta)$. By defining $\tilde{A} = A \cos(\delta)$ and using the approximation $B \sin(\delta) \approx 0$ the resulting equations simplify to

$$\left(\frac{\Gamma_i}{(1 + |\tilde{A}|^2)^2} - \gamma \right) \tilde{A} - igB = 0, \quad (\text{S26})$$

$$\left(-\frac{\Gamma_e}{(1 + |\tilde{A}|^2)^2} - \gamma \right) \tilde{A} + igB = 0. \quad (\text{S27})$$

Therefore, similar to above we obtain the amplitudes

$$|\tilde{A}|^2 = \sqrt{\frac{\Gamma_i - \Gamma_e}{2\gamma}} - 1, \quad B = -i\frac{\gamma}{g} \frac{\Gamma_i + \Gamma_e}{\Gamma_i - \Gamma_e} \tilde{A}, \quad (\text{S28})$$

and, since $\sin(k_0) = \cos(\delta)$, the identical current

$$\langle J \rangle = n_0 \gamma \frac{\Gamma_i + \Gamma_e}{\Gamma_i - \Gamma_e} \left(\sqrt{\frac{\Gamma_i - \Gamma_e}{2\gamma}} - 1 \right). \quad (\text{S29})$$

Symmetry-broken phase

We now consider the regime $\Gamma_i < \Gamma_e$. As a main difference we find that in this regime the choice of $k_0 = \frac{\pi}{2}$ leads to a stationary solution for even N , which obeys

$$\left(\frac{\Gamma_i}{(1 + |A|^2)^2} - \gamma \right) A - igB = 0, \quad (\text{S30})$$

$$\left(\frac{-\Gamma_e}{(1 + |B|^2)^2} - \gamma \right) B - igA = 0, \quad (\text{S31})$$

and $\omega = 0$. These equation have a solution for $\Gamma_e \geq \Gamma_i$, but not for $\Gamma_i > \Gamma_e$. Although these equations can still be still solved analytically, the results are already quite involved. However, sufficiently deep in the symmetry-broken phase we can neglect the bare decay γ and approximate $\Gamma_e(B) \approx \Gamma_e$. We then obtain

$$|A|^2 \simeq \sqrt{\frac{\Gamma_i}{\kappa + \frac{g^2}{\Gamma_e}}} - 1, \quad B \simeq -i\frac{g}{\Gamma_e} A, \quad (\text{S32})$$

and the current

$$\langle J \rangle \simeq \frac{g^2 n_0}{\Gamma_e} \left(\sqrt{\frac{\Gamma_i}{\kappa + \frac{g^2}{\Gamma_e}}} - 1 \right). \quad (\text{S33})$$

For N odd, the choice $k_0 = \pi/2$ would results in a symmetric steady-state and also the resulting equations for A and B do not have a solution for $\Gamma_i < \Gamma_e$. To recover a symmetry-broken solution with a maximal current we choose $\delta = \pi/(2N)$. In this case the chain undergoes persistent oscillations with frequency $\omega = g \sin(\delta)$. By defining $\tilde{A} = A \cos(\delta) - B \sin(\delta)$ the remaining equations simplify to

$$\left(\frac{\Gamma_i}{(1 + |\tilde{A}|^2)^2} - \gamma \right) \tilde{A} - igB = 0, \quad (\text{S34})$$

$$\left(\frac{-\Gamma_e}{(1 + |B|^2)^2} - \gamma \right) B - ig\tilde{A} = 0. \quad (\text{S35})$$

Therefore, as long as $B \sin(\delta) \ll 1$, we obtain analogous solutions and the identical current as in the case of an even number of oscillators.

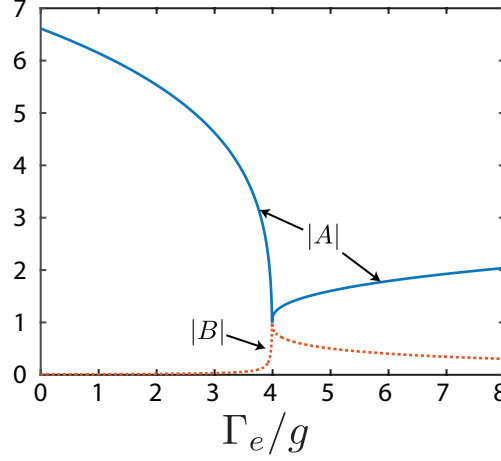


FIG. S4. The coefficients $|A|$ (solid line) and $|B|$ (dotted line) for a fixed injection strength $\Gamma_i = 4g$ as a function of the extraction strength Γ_e for a damping of $\gamma = 10^{-3}g$.

Symmetry breaking transition

In Fig. (S4) we plot the values of A and B for the whole range of Γ_e . We see that in both phases $|A| \gg |B|$, which corresponds to either a symmetric or asymmetric zig-zag structure of the chain. Only near the transition point we find $|A| \simeq |B|$. More precisely, from the solution in the symmetric regime we see that $B = -iA$, at a value of

$$\Gamma_e^* = \Gamma_i \frac{g - \gamma}{g + \gamma} \approx \Gamma_i - \frac{2\Gamma_i}{g}\gamma. \quad (\text{S36})$$

Near this parameter the standing wave turns into a running wave $\alpha_\ell^0 \sim e^{ik_0\ell}$ and the current is close to maximum and scales $\langle J \rangle_{\max} \propto \sqrt{\Gamma_i}$. Although the symmetric solution exists up to $\Gamma_e^{**} = \Gamma_i - 2\gamma$, the stability analysis reveals that for $\Gamma_i > g$ the symmetric solution becomes unstable before, at around $\Gamma \simeq \Gamma_e^*$. In the regime of interest, $\gamma/g \rightarrow 0$, these differences become negligible and the transition is simply given by $\Gamma_e \simeq \Gamma_i$.

Damping of all oscillators

The results derived so far for a chain without damping of the oscillators in the middle agree in essence with the results of obtained for two coupled oscillators (see also Ref. [S7]). However, while in the symmetry-broken phase the bare damping γ has a negligible effect, it determines the value of the current in the symmetric phase. In this regime it is thus important to analyze the steady state also for the full system, where all oscillators are weakly damped. In this case the equation

$$\dot{\alpha}_\ell = -\frac{\gamma}{2}\alpha_\ell + i\frac{g}{2}(\alpha_{\ell-1} + \alpha_{\ell+1}), \quad (\text{S37})$$

cannot be fulfilled by the ansatz (S17). However, for $\gamma/g \ll 1$ the correction are small and we can still use this ansatz with the same k_0 as above as a first approximation. For simplicity we focus on N odd where $k_0 = \frac{\pi}{2}$. Then, summing the equations for every other site we obtain

$$\sum_{\ell=1}^{(N-1)/2} (-1)^{\ell+1} \dot{\alpha}_{2\ell-1} = \sqrt{n_0} \left(\Gamma_i(A)A - \gamma \sum_{\ell=1}^{(N-1)/2} A - igB \right) = 0, \quad (\text{S38})$$

and for the last site,

$$\dot{\alpha}_N = \sqrt{n_0} [(-\Gamma_e(A) - \gamma)A + igB] = 0. \quad (\text{S39})$$

Therefore, we find following solutions for the amplitudes

$$|A|^2 = \sqrt{\frac{2(\Gamma_i - \Gamma_e)}{\gamma(N+1)}} - 1, \quad B = -i\frac{\gamma}{2g} \frac{\Gamma_e(N-1) + 2\Gamma_i}{\Gamma_i - \Gamma_e} A, \quad (\text{S40})$$

and for the current

$$\langle J \rangle = n_0 \frac{\gamma}{2} \frac{\Gamma_e(N-1) + 2\Gamma_i}{\Gamma_i - \Gamma_e} \left(\sqrt{\frac{2(\Gamma_i - \Gamma_e)}{\gamma(N+1)}} - 1 \right). \quad (\text{S41})$$

Note that although the result was derived for N odd, it is a good approximation for N even for $N > 2$.

Symmetry breaking

In steady state the total energy of the system must be conserved, i.e. the absorbed and dissipated energy must be the same,

$$\Gamma_i(\alpha_1^0)|\alpha_1|^2 = \Gamma_e(\alpha_N^0)|\alpha_N^0|^2 + \gamma \sum_{\ell=1}^N |\alpha_\ell^0|^2. \quad (\text{S42})$$

For a symmetric state, where $|\alpha_1^0| = |\alpha_N^0| = \alpha^0$, and $|\alpha_\ell^0|^2 = \eta_\ell |\alpha^0|^2$ we obtain

$$\Gamma_i(\alpha^0) - \Gamma_e(\alpha^0) = \gamma \mathcal{N}, \quad \mathcal{N} = \sum_{\ell=1}^N \eta_\ell, \quad (\text{S43})$$

where $\mathcal{N} = 2$ for $N = 2$, $\mathcal{N} \simeq (N+1)/2$ for N odd and in general $\mathcal{N} \approx N/2$ for $N \gg 1$. By increasing the value of α^0 , this condition can always be satisfied as long as $\Gamma_e < \Gamma_i - \gamma \mathcal{N}$, which represent a minimal condition for the existence of a symmetric phase. However, similar as above, one find that for $\Gamma_i > g$ symmetry breaking already occurs closer to the point where $|A| = |B|$ and we find the transition point approximately at

$$\Gamma_e^* = \frac{2\Gamma_i(g - \gamma)}{2g + \gamma(N-1)}. \quad (\text{S44})$$

As long as $\gamma N \ll g$, the transition point does not considerable change by changing the system size and for all results presented in the main text the transition point at $\Gamma_e \simeq \Gamma_i$ is a sufficient approximation.

Note that near Γ_e^* we obtain a single traveling wave. To account first order corrections due to a finite decay $\gamma/g \ll 1$, we can generalize the ansatz to $\alpha_\ell^0 \sim e^{ik_0 \ell} e^{-\kappa \ell}$. From Eq. (S37) we then obtain $\kappa = \gamma/(2g)$. Therefore, all our analytic estimates will remain valid as long as $N\gamma \ll 1$, although numerical simulations show that most of the qualitative features survive at much larger decay rates.

CURRENT FLUCTUATIONS IN THE THERMAL REGIME

In regime of large thermal noise, $n_0 \gg 1$ and $N_{\text{th}}/n_0 > 1$ the system can no longer be solved analytically. To obtain approximate results for the current fluctuations in the symmetric and the symmetry-broken regime, we consider a minimal system with $N = 2$ oscillators, for which the relevant scalings can be derived. Our numerical simulations show that these results do not considerable change for larger chains.

Equilibrium fluctuations

We first consider the two coupled oscillators in thermal equilibrium, where $\Gamma_i = \Gamma_e = 0$. In this case we get a closed set of equations for the variances of the linear chain, which can be evaluated assuming a thermal state $\rho_{\text{th}} = \rho_{\text{th}}^1 \otimes \rho_{\text{th}}^2$. We obtain

$$\begin{aligned} \frac{(\Delta J)^2}{n_0^2} &= \frac{g^2}{4n_0^2} \left[\langle a_\ell^\dagger a_\ell a_{\ell+1} a_{\ell+1}^\dagger + a_\ell a_\ell^\dagger a_{\ell+1}^\dagger a_{\ell+1} - a_\ell a_\ell a_{\ell+1}^\dagger a_{\ell+1}^\dagger - a_\ell^\dagger a_\ell^\dagger a_{\ell+1} a_{\ell+1} \rangle - \langle a_\ell^\dagger a_{\ell+1} - a_\ell a_{\ell+1}^\dagger \rangle^2 \right] \\ &= \frac{g^2}{4n_0^2} \left[\langle a_\ell^\dagger a_\ell \rangle \langle a_{\ell+1} a_{\ell+1}^\dagger \rangle + \langle a_\ell a_\ell^\dagger \rangle \langle a_{\ell+1}^\dagger a_{\ell+1} \rangle \right] = \frac{g^2}{4n_0^2} 2(N_{\text{th}}^2 + N_{\text{th}}) \approx \frac{g^2}{2} \left(\frac{N_{\text{th}}}{n_0} \right)^2. \end{aligned} \quad (\text{S45})$$

Symmetric regime

For $\Gamma_e < \Gamma_i$ the system is strongly influenced by thermal fluctuations. By calculating the expectation values of higher order moments we can find approximate solutions for the mean occupation and their fluctuations. For $\gamma/g \ll 1$, we can approximate $\Gamma(\alpha) = \frac{\Gamma}{(1+|\alpha|^2/n_0)^2} \approx \frac{\Gamma n_0^2}{|\alpha|^4}$ and arrive at following equation of motion

$$\langle |\dot{\alpha}_1|^2 + |\dot{\alpha}_2|^2 \rangle = \left\langle \frac{\Gamma_i n_0^2}{|\alpha_1|^2} - \frac{\Gamma_e n_0^2}{|\alpha_2|^2} \right\rangle - \gamma(\langle |\alpha_1|^2 \rangle + \langle |\alpha_2|^2 \rangle) + 2\gamma N_{\text{th}} = 0. \quad (\text{S46})$$

In the symmetric regime $\langle |\alpha_1|^2 \rangle = \langle |\alpha_N|^2 \rangle$ and by approximating $\langle \frac{1}{|\alpha|^2} \rangle \approx \frac{1}{\langle |\alpha|^2 \rangle}$, we obtain

$$\frac{\langle |\alpha_1|^2 \rangle}{n_0} = \frac{\langle |\alpha_2|^2 \rangle}{n_0} \approx \sqrt{\frac{\Gamma_i - \Gamma_e}{2\gamma} + \left(\frac{N_{\text{th}}}{2n_0}\right)^2} + \frac{N_{\text{th}}}{2n_0} \approx \frac{N_{\text{th}}}{n_0} + \sqrt{\frac{\Gamma_i - \Gamma_e}{2\gamma}}. \quad (\text{S47})$$

By assuming that the noise doesn't considerable change the mean value of the relative phase and just broadens the phase distribution, we can approximate the mean current by

$$\langle J \rangle \approx n_0 \gamma \frac{\Gamma_i + \Gamma_e}{\Gamma_i - \Gamma_e} \left(\sqrt{\frac{\Gamma_i - \Gamma_e}{2\gamma}} + \frac{N_{\text{th}}}{n_0} \right). \quad (\text{S48})$$

Therefore, for $\gamma/g \ll 1$ and not too large thermal noise the mean current is hardly affected by thermal fluctuations, which agrees very well with numerical simulations.

The variances of $|\alpha_\ell|^2$ can be calculated from the equations of motion for higher moments. For the occupation fluctuations we obtain

$$\langle |\dot{\alpha}_1|^4 + |\dot{\alpha}_2|^4 \rangle = 2(\Gamma_i - \Gamma_e)n_0^2 - 2\gamma(\langle |\alpha_1|^4 \rangle + \langle |\alpha_2|^4 \rangle) + 4\gamma N_{\text{th}}(\langle |\alpha_1|^2 \rangle + \langle |\alpha_2|^2 \rangle) = 0. \quad (\text{S49})$$

In the symmetric regime $\langle |\alpha_1|^n \rangle = \langle |\alpha_2|^n \rangle$ and using Eq. (S47), we find

$$\begin{aligned} \langle |\alpha_1|^4 \rangle &\approx \frac{(\Gamma_i - \Gamma_e)n_0^2}{2\gamma} + 2N_{\text{th}}\langle |\alpha_1|^2 \rangle = \frac{(\Gamma_i - \Gamma_e)n_0^2}{2\gamma} + 2N_{\text{th}}\langle |\alpha_1|^2 \rangle \\ &= \frac{(\Gamma_i - \Gamma_e)n_0^2}{2\gamma} + 2N_{\text{th}} \left(\sqrt{\frac{(\Gamma_i - \Gamma_e)n_0^2}{2\gamma} + \left(\frac{N_{\text{th}}}{2}\right)^2} + \frac{N_{\text{th}}}{2} \right), \end{aligned} \quad (\text{S50})$$

and for the variance

$$\frac{\text{Var}(|\alpha_\ell|^2)}{n_0^2} \approx \frac{N_{\text{th}}}{n_0} \left(\sqrt{\frac{\Gamma_i - \Gamma_e}{2\gamma} + \left(\frac{N_{\text{th}}}{2n_0}\right)^2} + \frac{N_{\text{th}}}{2n_0} \right) = \frac{N_{\text{th}}}{n_0} \frac{\langle |\alpha_\ell|^2 \rangle}{n_0}. \quad (\text{S51})$$

In the regime $\gamma/g \ll 1$, the occupation $\langle |\alpha_i|^2 \rangle$ is hardly affected by the thermal noise and the variance depends linearly on N_{th} . Furthermore, we can approximate the variance of the current by

$$\begin{aligned} \frac{\text{Var}(\langle J \rangle)}{g^2 n_0^2} &\approx \langle |\alpha_1|^2 \rangle \text{Var}(|\alpha_N|^2) + \langle |\alpha_N|^2 \rangle \text{Var}(|\alpha_1|^2) + \text{Var}(|\alpha_1|^2) \text{Var}(|\alpha_N|^2) \\ &\approx \frac{2N_{\text{th}}\langle |\alpha_1|^2 \rangle + N_{\text{th}}^2}{n_0^2}, \end{aligned} \quad (\text{S52})$$

where we again observe linear dependence on N_{th} in the limit of $\gamma/g \ll 1$ and $\langle |\alpha_1|^2 \rangle \gg N_{\text{th}}$. Again, this approximate result reproduces well all our numerical findings.

Symmetry-broken regime

For $\Gamma_e > \Gamma_i$ we find that in steady state $\Gamma_e(\alpha_2^0) \approx \Gamma_e$. By making this approximation we can linearize around the steady state amplitude and obtain the following expression for the variance of the current in the limit of $\gamma \rightarrow 0$,

$$\frac{\text{Var}(\langle J \rangle)}{n_0^2} = \gamma N_{\text{th}} g^2 \frac{(\sqrt{\Gamma_i \Gamma_e} - g) [g^2 (4g - 5\sqrt{\Gamma_i \Gamma_e}) + \Gamma_e (\Gamma_e \sqrt{\Gamma_i \Gamma_e} + 2\Gamma_i g)]}{\Gamma_e (\sqrt{\Gamma_i \Gamma_e} - 2g) [\Gamma_e^2 \sqrt{\Gamma_i \Gamma_e} + g^2 (4g - 3\sqrt{\Gamma_i \Gamma_e})]}. \quad (\text{S53})$$

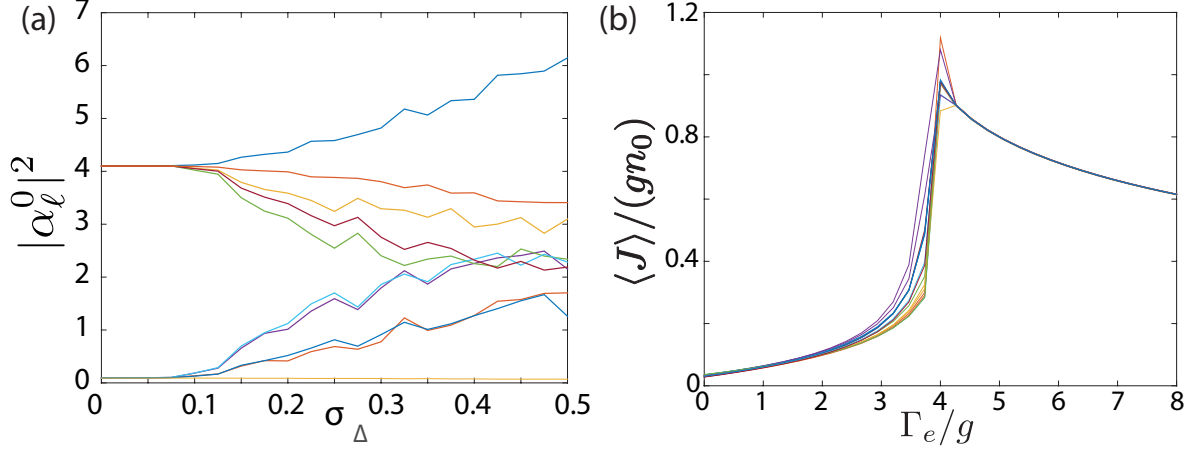


FIG. S5. (a) Plot of the occupation numbers $|\alpha_\ell^0|^2$ averaged over 100 realizations of random detunings $\Delta_\ell \in [-\sigma_\Delta, \sigma_\Delta]$ for a chain of $N = 10$ oscillators with gain $\Gamma_i = 4g$, loss $\Gamma_e = 8g$ and damping $\gamma/g = 10^{-3}$. (b) Current for 15 different random detuning realizations with $\sigma_\Delta = 0.05g$.

We see that for small damping rate γ , the fluctuations of the current are small. In particular, deep in the symmetry-broken phase,

$$\frac{\text{Var}(\langle J \rangle)}{n_0^2} \approx \frac{\gamma N_{\text{th}} g^2}{\Gamma_e}, \quad \frac{\Delta J}{J} \approx \sqrt{\frac{\gamma N_{\text{th}} (\gamma \Gamma_e + g^2)}{g^2 \Gamma_i}}. \quad (\text{S54})$$

DISORDER

For all our results presented in the main part of the paper, we have considered chains of oscillators with identical frequencies $\omega_\ell = \omega_0$. To understand the robustness of the observed effects with respect to small frequency variations, which will be unavoidable in any real system, we numerically simulate the steady state of a chain of $N = 10$ oscillators with frequencies $\omega_\ell = \omega_0 + \Delta_\ell$. Here the random frequency offsets are chosen from a uniform distribution σ_Δ , i.e., $\Delta_\ell \in [-\sigma_\Delta, \sigma_\Delta]$.

In Fig. S5 (a) and (b) we plot the disorder-averaged steady-state occupation numbers $|\alpha_\ell^0|^2$ for each of the oscillators and the current for a few disorder realizations. We find that for $\sigma_\Delta < 0.1g$, the steady state amplitudes reproduce almost perfectly the alternating structure predicted for the ideal case, $\Delta_\ell = 0$. In this regime also the current exhibits the characteristic peak structure for each individual disorder realization and is hardly affected for parameters away from the transition point. This shows that all the effects discussed in the main part of this work are insensitive to a small amount of disorder. For $0.1 < \sigma_\Delta/g < 0.3$, the amplitudes still follow more or less a zig-zag structure, while for $\sigma_\Delta/g > 0.3$ the occupation structure is completely different from the non-detuned case and most of the energy gets localized around the gain mode. Details about this localization transition are subject of ongoing research and will be presented elsewhere.

UNIVERSALITY OF THE SYMMETRY-BREAKING TRANSITION

For all the results discussed in the main text we have assumed a specific cutoff function and the same saturation occupation number n_0 for the gain and the loss mechanism. While the precise quantitative findings will of course depend on these assumptions, we will now demonstrate with several other examples that the most important qualitative features of the energy transport do not depend on these details.

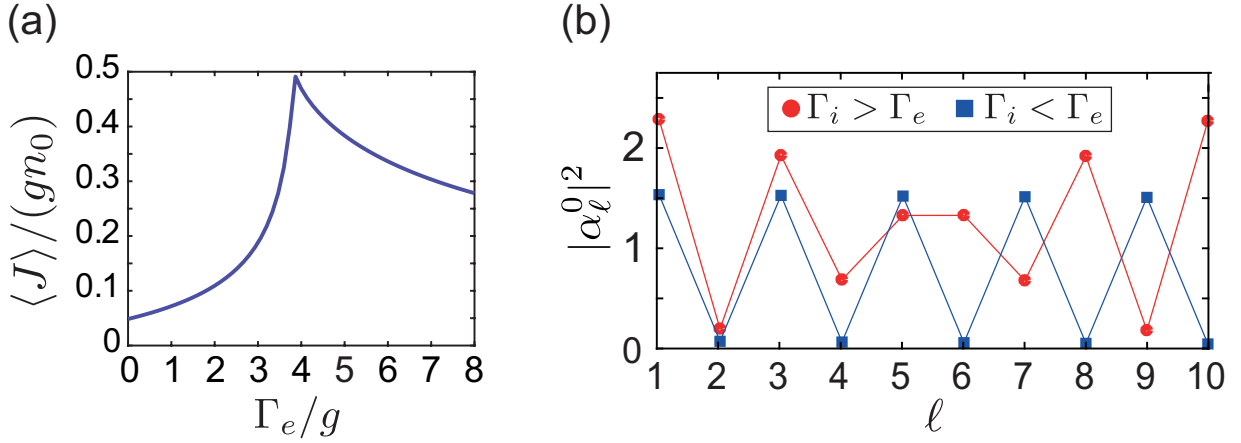


FIG. S6. Current for fixed injection rate $\Gamma_i = 4g$ as function of the extraction rate Γ_e for a non-linearity of the gain/loss mechanism $\nu = 3$ and a damping rate $\gamma/g = 10^{-2}$. b) Occupation structure of a chain of $N = 10$ oscillators for a injection rate of $\Gamma_i = 4g$ and a extraction rate of $\Gamma_e = 2$ (red) and $\Gamma_e = 6$ (blue).

Different gain/loss mechanisms

As there are many ways to engineer gain and loss, we first show that our findings do not depend on the precise form of the saturation function $f(x)$. In Fig. (S6) we consider the example of a cutoff function defined in Eq. (S4) with $\nu = 3$ to model a system with a stronger saturation dependence. We see that although the current and the steady-state occupation numbers are substantially lower, the sharp maximum and the transition from a symmetric to a symmetry-broken regime are still clearly visible. Also in the presence of noise, [see Fig. S8(b) below], this transition is associated with a strong reduction of noise and a finite value of the order parameter $\bar{\Gamma} = \langle \Gamma_e(\alpha_N) - \Gamma_i(\alpha_1) \rangle$. Further, in Fig. S6(b) we find that in steady state the system is determined by a single mode with the same wavevector k_0 as for $\nu = 2$.

In Fig. (S7) we also consider the case of a weaker saturation dependence, i.e., $\nu = 1$. This case corresponds to the saturation dependence for a regular laser. Again we see that the general structure of the current with a maximum at $\Gamma_e \simeq \Gamma_i$ is reproduced. However, for $\Gamma_i \gtrsim 3.4g$ we obtain a region, where the current does not have a precise value and the whole chain settles into a limit cycle. Such a behavior has previously been predicted for the PT-symmetric case $\Gamma_i = \Gamma_e$, where $\nu = 1$ has been identified as a special case, where no real symmetry-breaking occurs. The current analysis shows that this is only true within a small region around the transition point. In the presence of thermal noise [see Fig. S8(a)] these limit cycles are no longer visible and we obtain again the same transition with a strong reduction of noise and a finite value of the order parameter $\bar{\Gamma} = \langle \Gamma_e(\alpha_N) - \Gamma_i(\alpha_1) \rangle$.

Different saturation numbers n_0

To further show that the physical effects shown in the main text are very generic, we also consider the case where the gain and the loss oscillator saturate at different amplitudes $n_0^{(1)} \neq n_0^{(N)}$. This removes any residual symmetry in the equations of motion. The resulting mean currents and fluctuations are shown in Fig. (S9) and Fig. (S10). We still observe all the qualitative features of the symmetry-breaking phase transition, except that the symmetry breaking point is now shifted from $\Gamma_i = \Gamma_e$ to $\Gamma_i = \Gamma_e(n_0^{(N)}/n_0^{(1)})^2$ (in the limit $\gamma/g \ll 1$). For $N_{th} > n_0$, this transition is again associated with a strong reduction of noise and the emergence of a finite value of the order parameter $\bar{\Gamma} = \langle \Gamma_e(\alpha_N) - \Gamma_i(\alpha_1) \rangle$, which indicates the symmetry-breaking.

NUMERICAL SIMULATIONS

For the numerical results presented in Fig. 3, and Fig. 4(a) ($n_0 = 10, 30$) and Fig. 5 in the main text we have simulated the stochastic equations Eqs. (3)-(5) of the main text using the Euler Maruyama method with a timestep of $\Delta t = 10^{-4}g$. For efficient simulation with Matlab, we vectorize the equations and simultaneously time evolve

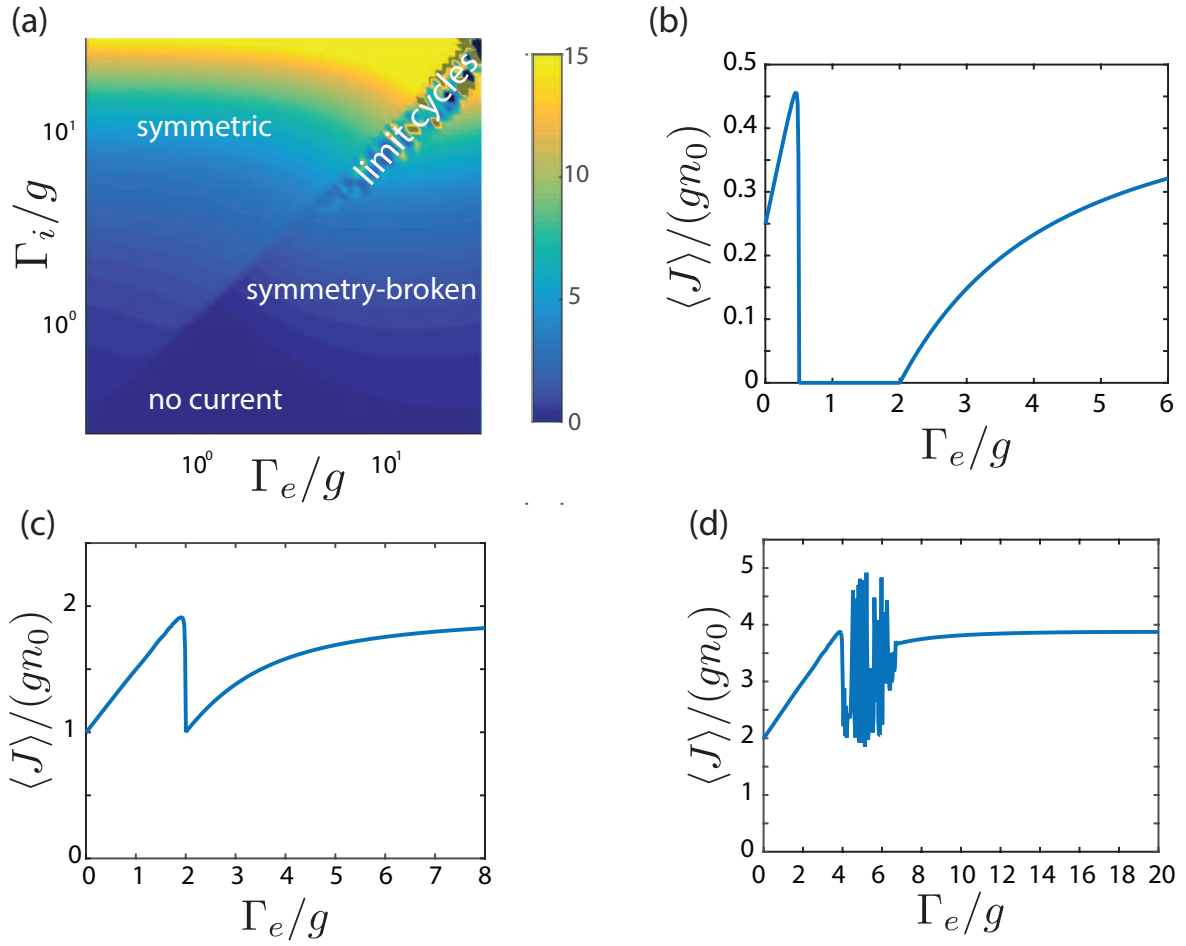


FIG. S7. (a) Phase diagram for a non-linearity of the gain/loss mechanism of $\nu = 1$ as a function of the injection strength Γ_i and the extraction strength Γ_e and for a damping rate $\gamma = 10^{-2}g$. Current as a function of the extraction strength Γ_e for fixed injection strength (b) $\Gamma_i = 0.5g$, (c) $\Gamma_i = 2g$ and (d) $\Gamma_i = 4g$ and for a damping rate $\gamma = 10^{-3}g$.

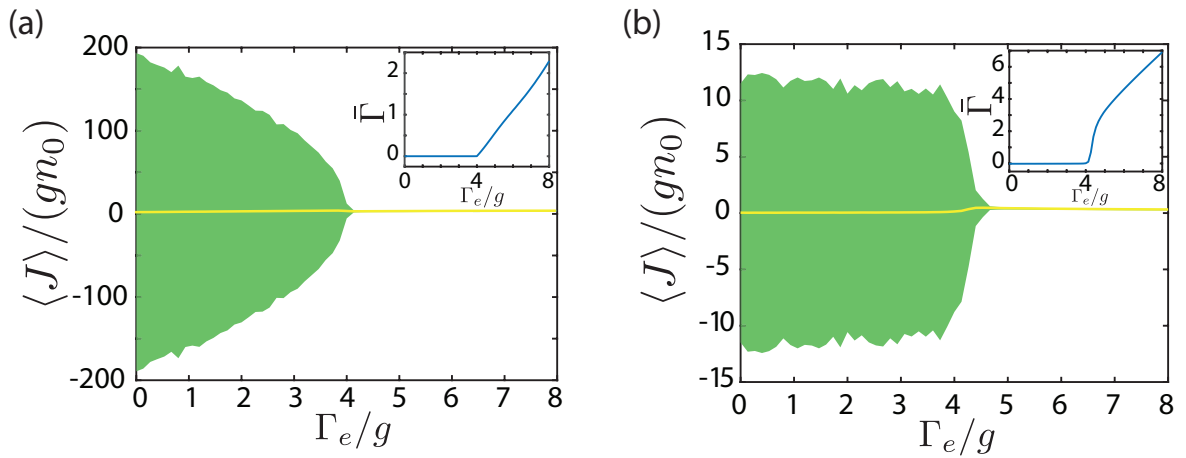


FIG. S8. Current for fixed injection rate $\Gamma_i = 4g$ as function of the extraction rate Γ_e for a non-linearity of the gain/loss mechanism of (a) $\nu = 1$ and (b) $\nu = 3$ when the whole system is coupled to a thermal bath with the rate $\gamma/g = 10^{-3}$ and the temperature $N_{th}/n_0 = 10$.

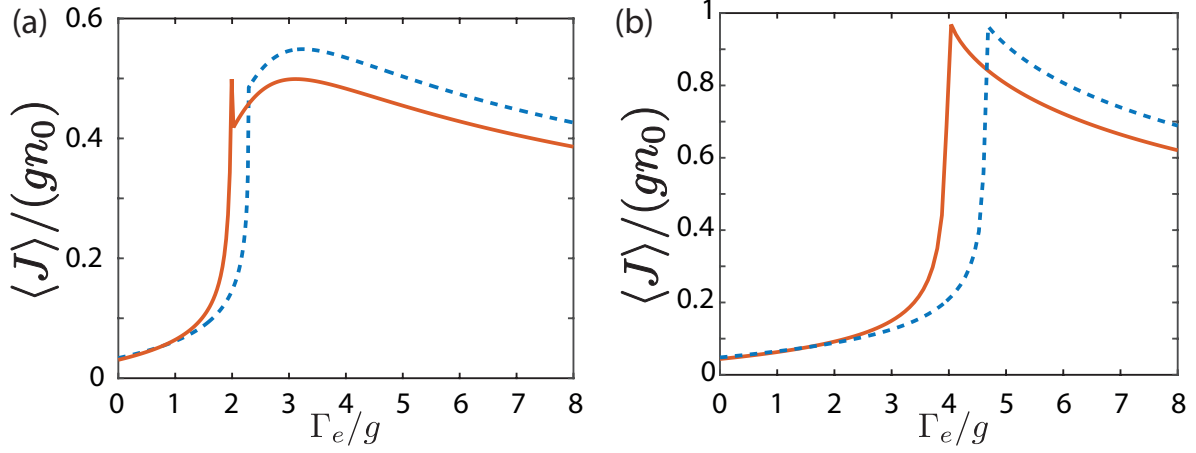


FIG. S9. Current for fixed injection rate $\Gamma_i = 2$ (a) and $\Gamma_i = 4$ (b) as function of the extraction rate Γ_e , when the saturation numbers are equal $n_0^{(1)} = n_0^{(N)}$ (red solid line) and 10% different $n_0^{(1)} = 1.1n_0^{(N)}$ (blue dashed line) for a damping rate $\gamma = 10^{-3}g$.

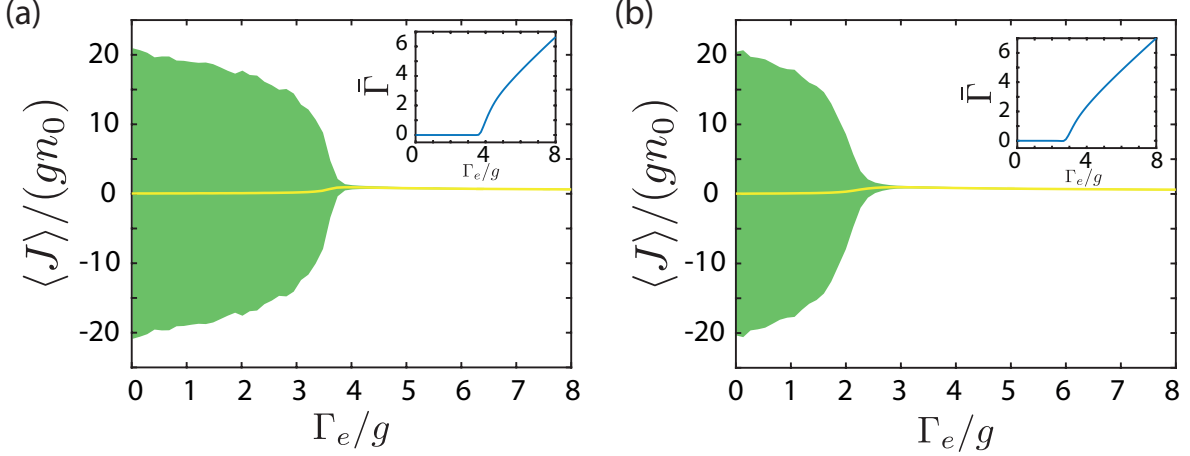


FIG. S10. Current for fixed injection rate $\Gamma_i = 4g$ as function of the extraction rate Γ_e for a non-linearity of the gain/loss mechanism of $\nu = 2$ and different saturation numbers (a) $n_0^{(N)} = 1.1n_0^{(1)}$ (b) $n_0^{(N)} = 1.5n_0^{(1)}$. The full system is coupled to a thermal bath with the rate $\gamma/g = 10^{-3}$ and a thermal occupation number of $N_{\text{th}}/n_0 = 10$.

$n_{\text{traj}} = 50$ trajectories at the same time. After $t = 5000g \approx 5\tau_r$, we sample every 17000 timestep for 3000 points per trajectory to get the steady state distribution.

For the cases $n_0 = 1, 2, 5$ in Fig. 4(a) and (b) of the main text we have used a stochastic quantum wavefunction method [S8, S9], to simulate the full master equation Eq. (S1). The results for $n_0 = 1$ were independently verified by calculating directly the steady-state density operator for a system of two coupled oscillators with $n_{\text{basis}} = 30$ basis states per oscillator. For the quantum trajectory simulation the evolution under the effective non-hermitian Hamiltonian has been implemented by the time evolution operator $U = e^{-iH_{\text{eff}}\Delta t}$ with $\Delta t = 2 \times 10^{-3}g$, which has to be computed once at the beginning of the trajectory. After random times quantum jumps occur and the state gets renormalized. After $t = 10000g \approx 10\tau_r$, when the system has for sure reached the steady state, we sample the state after every 800 timesteps for 990000 times to obtain the steady state density matrix. In Fig. 4(a) of the main text we used $n_{\text{basis}} = 70$ and $n_{\text{basis}} = 150$ states per oscillator for $n_0 = 1$ and $n_0 = 2$ while in Fig. 4(b) we used $n_{\text{basis}} = 30, 60, 100$ states per oscillator for $n_0 = 1, 2, 3$. The entanglement negativity was obtained by calculating the $4n_{\text{basis}}$ lowest eigenvalues after partial transpose.

The relaxation time in Fig. 4(c) in the main text was obtained by in the absence of noise, by first determining the steady state amplitudes with high accuracy. This was implemented by a 4-th order Runge-Kutta algorithm with an accuracy of 10^{-11} . Then the amplitude of the gain oscillator is changed by $\delta\alpha_1 = 1/10$ and the time evolution is performed until the system relaxes. From the time difference Δt_r between the pint where the occupation is just

$\delta|\alpha_1|^2 = 10^{-5}$ and $\delta|\alpha_1|^2 = 10^{-8}$ away from the real steady state, we obtain the relaxation rate as $\tau_r = \Delta t_r / \ln(10^3)$. Note that in Fig. 4(c) the relaxation rate exhibits a peak in a very small region around the transition point $\Gamma_e = \Gamma_i$, where we find almost no relaxation. In this regime the numerically extracted values for τ_r depend on very fine details and are no longer meaningful.

-
- [S1] D. F. Walls, and G. J. Milburn, *Quantum Optics* (Springer, 1994).
 - [S2] C. W. Gardiner and P. Zoller, *Quantum Noise*, (Springer, 2000).
 - [S3] K. V. Keesidis, S. D. Bennett, S. Portolan, M. D. Lukin, and P. Rabl, Phonon Cooling and Lasing with Nitrogen-Vacancy Centers in Diamond, *Phys. Rev. B* **88**, 064105 (2013).
 - [S4] E. C. G. Sudarshan, Equivalence of semiclassical and quantum mechanical descriptions of statistical light beams, *Phys. Rev. Lett.*, **10**, 277 (1963).
 - [S5] C. Gardiner, *Stochastic methods* (Springer, Berlin, 2009).
 - [S6] J. M. Vargas-Martínez, H. Moya-Cessa, and M. Fernández Guasti, Normal and anti-normal ordered expressions for annihilation and creation operators, *Revista mexicana de física E*, **52**, 13 (2006).
 - [S7] A. U. Hassan, H. Hodaei, M. A. Miri, M. Khajavikhan, and D. N. Christodoulides, Nonlinear reversal of the PT-symmetric phase transition in a system of coupled semiconductor microring resonators, *Phys. Rev. A* **92**, 63807 (2015).
 - [S8] J. Dalibard, Y. Castin, and K. Mølmer, Wave-function approach to dissipative processes in quantum optics, *Phys. Rev. Lett.*, **68**, 580 (1992).
 - [S9] A. J. Daley, Quantum trajectories and open many-body quantum systems, *Advances in Physics*, **63**, 77 (2014).